

Fluid Mechanics Report:
Aerodynamic Behaviors in Hele-Shaw Flow

MAE 171A
Professors Jan Kleissl, Marko Lubarda, Alessandro Marinoni



Team Members:

Ravi Harun
Rayyan Khalid
Alice Khalil
Tanmay Prakash

I. ABSTRACT

In our study, we investigated the behavior of Hele-Shaw flow around various objects using a modified apparatus designed to replicate quasi-two-dimensional flow conditions. By visualizing the flow with dyed fluids between two parallel plates, we analyzed the effects of structural changes on fluid dynamics, specifically focusing on cylindrical objects and a NACA 8612 airfoil equipped with leading-edge slats. This approach allowed us to directly observe phenomena such as flow separation and stagnation points, providing empirical support to theoretical models. Our results provide empirical validation of theoretical models and reveal the significant influence of geometric alterations on fluid behavior. Notably, the introduction of leading-edge slats on airfoils demonstrated a marked improvement in delaying stall by maintaining lift at higher angles of attack, thereby offering practical insights into aerodynamic optimization. This study offers significant insights into optimizing aerodynamic surfaces, demonstrating the practical application of Hele-Shaw flow principles in both academic research and industrial design.

II. INTRODUCTION

Fluid dynamics explores fluid behavior under various influences, which is crucial across numerous scientific and engineering applications [1]. Hele-Shaw flow, which involves fluid moving between two narrowly spaced plates, is vital for understanding fluid behavior in constrained environments and has significant applications from engineering to environmental studies [2]. However, there remains a critical need for empirical data to support theoretical and computational models, particularly in practical engineering scenarios like aerodynamics.

This report aims to bridge the gap between theoretical frameworks and practical applications by providing detailed visualizations of fluid flow around common engineering shapes, such as cylinders and airfoils with leading-edge slats. Our experiments not only allowed for direct observation of fluid dynamics phenomena like streamlines and stagnation points, but also tested the effectiveness of leading-edge slats in improving airfoil efficiency at high attack angles. By integrating hands-on experiments with theoretical analysis, this study offers insights into how structural modifications can impact fluid flow, enhancing our understanding of nearly two-dimensional fluid dynamics and suggesting ways to optimize aerodynamic designs.

Our experiments focused on two fundamental flow cases: an airfoil at a high angle of attack (AoA) and a Rankine half-body. The airfoil experiments particularly explored boundary layer separation and stall, critical phenomena that limit the operational range of aircraft wings. Meanwhile, the Rankine half-body, an idealized scenario, allowed for comparisons between experimental observations and potential flow theory predictions. Together, these experiments underline the importance of marrying theoretical models with experimental validation to refine fluid mechanics understanding and aerodynamic applications.

Through this research, we aim to refine fluid dynamics models and develop more efficient and effective aerodynamic structures, contributing valuable insights to both theoretical knowledge and practical design.

III. PROCEDURES

The experiment utilized a Hele-Shaw flow table to visualize quasi-two-dimensional, low Reynolds number flow around various objects, such as cylinders and airfoils. The setup included two parallel glass plates with a small gap for water flow, enhanced by food coloring injections to highlight streamlines. We controlled the flow rate at 0.8 GPM using a rotameter, adjusting the water level and food coloring valve to minimize disturbances before each test. We analyzed the flows considering the assumptions mentioned in the A3 of the appendix.

Initially, we observed baseline flow characteristics around simple shapes: undisturbed flow, a 4.5-inch diameter cylinder, and Rankine half- and full-body configurations, using a mix of source and sink elements to simulate flow. We recorded flow rates and captured images for analysis to establish theoretical comparisons.

The study's second phase focused on an airfoil at increasing angles of attack to identify boundary layer separation and stall points. We began without a leading-edge slat to set a baseline for the stall angle, documenting lift forces and the critical stall-indicating flow separations. We then introduced a 5" x 3" leading-edge slat, adjusted to delay stall, and repeated the visualization to observe changes in flow attachment and separation. This structured exploration provided deep insights into fluid dynamics principles such as stagnation points and wake formation, bridging theoretical predictions with empirical observations.

IV. RESULTS

We will investigate steady quasi-two-dimensional, low Reynolds number flow around various objects using a modified version of the gunt HM152 flow table. The experiments were structured to explore flow phenomena around a cylinder, Rankine half- and full-body, and an airfoil at high angles of attack, both with and without a leading-edge slat. We will then extend this results section by discussing analytically and experimentally obtained analysis (for Rankine half body, airfoil and airfoil with edge slat).

IV.1. Preliminary Calculations

The Reynolds number (Re) was calculated for each flow scenario around the objects [3]:

$$Re = \frac{\rho \cdot U \cdot L}{\mu}$$

where ρ is the fluid density, U the flow velocity, L the characteristic length, and μ the dynamic viscosity. The fluid density was taken to be 997 kg/m^3 and the dynamic viscosity as $1.002 \times 10^{-3} \text{ N.s/m}^2$.

The characteristic length was chosen based on the geometry of each object, allowing for comparisons between different setups. We calculated the flow velocity using the volumetric flow rate that we set using the supply tank valve. First we calculate the volumetric flow rate, Q :

$$Q = 0.8 \text{ gal/min} = 5.0472 \times 10^{-5} \text{ m}^3/\text{s}$$

Manipulating the formula for volume flow rate we can get the flow velocity as shown

$$U = \frac{Q}{A}$$

where U is the velocity and A is the cross-sectional area [1].

Cross-sectional area can be calculated by the width and the depth of the plates which were 0.585 m and 0.005 m, respectively. So, the area is:

$$A = 0.585 \times 0.005 = 2.925 \times 10^{-3} \text{ m}^2$$

Now, plugging in these values, we get the uniform flow velocity to be:

$$U = \frac{5.0472 \times 10^{-5}}{2.925 \times 10^{-3}} = 0.0173 \text{ m/s}$$

Now, we will start displaying the results for each all four classic flow scenarios.

IV.2. Undisturbed Flow

For the undisturbed flow [A2], we chose characteristic length to be the gap width between the two plates. Thereby, the Reynolds number calculation will be:

$$Re = \frac{997 \times 0.0173 \times 0.005}{1.002 \times 10^{-3}} = 86.068$$

IV.3. Cylinder

The diameter of the cylinder [A3], which was 0.1143 m, served as the characteristic length for the Reynolds number calculation of the cylinder.

$$Re = \frac{997 \times 0.0173 \times 0.1143}{1.002 \times 10^{-3}} = 1967.523$$

IV.4. Rankine Full Body

A Rankine full-body is formed by superimposing a source, a sink, and a uniform flow. The flow has a closed streamline that forms the body [A4]. The characteristic length for a rankine full-body is typically between the source and the sink, 0.2268 m in our case. So, the Reynolds number is

$$Re = \frac{997 \times 0.0173 \times 0.2268}{1.002 \times 10^{-3}} = 3904.061$$

IV.5. Rankine Half Body

IV.5.1 Reynolds Number Calculation

A Rankine half-body is formed by superimposing a source and a uniform flow. [Fig 1.1] The flow has a stagnation point and a dividing streamline that separates the flow from the source and the uniform flow as indicated in Figure 1.1. The characteristic length is typically represented by the distance from the source to the stagnation point. This distance is given as:

$$L = \frac{m}{2\pi U}$$

Where m is the source strength (volume flow rate per unit depth) and U is the velocity of the uniform flow. The source strength m definition is:

$$m = \frac{\text{source flow rate}}{\text{depth}} = \frac{1.5773 \times 10^{-6}}{0.005} = 3.1546 \times 10^{-4} \text{ m}^2/\text{s}$$

So, the Reynolds number calculation for a rankine half-body will be as follows:

$$Re = \frac{\rho U L}{\mu} = \frac{\rho U \frac{m}{2\pi U}}{\mu} = \frac{\rho m}{2\pi \mu} = \frac{997 \times 3.1546 \times 10^{-4}}{2\pi \times 1.002 \times 10^{-3}} = 49.956$$

IV.5.2 Analytical and Numerical Results

The velocity magnitude contour [Fig. 1.4] confirms the expected Rankine flow behavior, where the freestream velocity smoothly transitions around the half-body with minimal separation. The particle pathlines [Fig. 1.2] exhibit symmetrical streamlines, reinforcing the theoretical assumption that potential flow analysis can effectively approximate this case. The static pressure contours [Fig. 1.3] show an increase in pressure near the stagnation point, with a gradual recovery downstream.

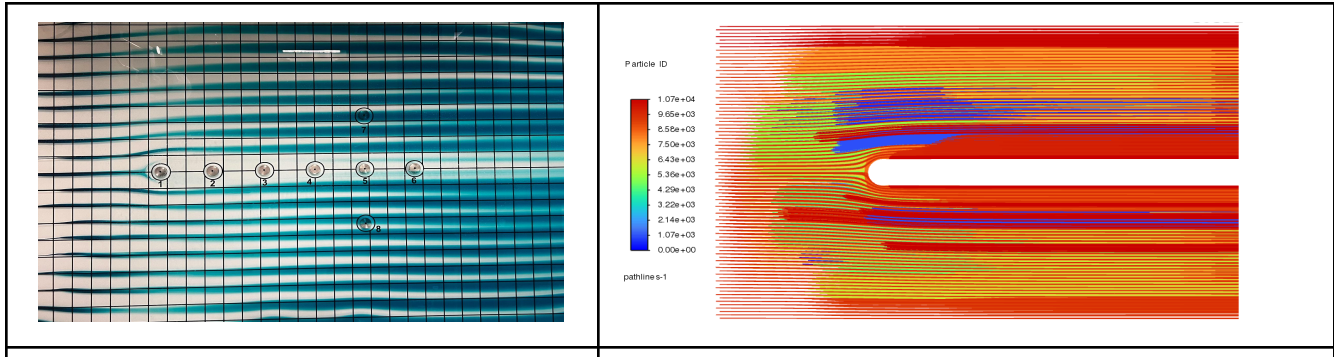
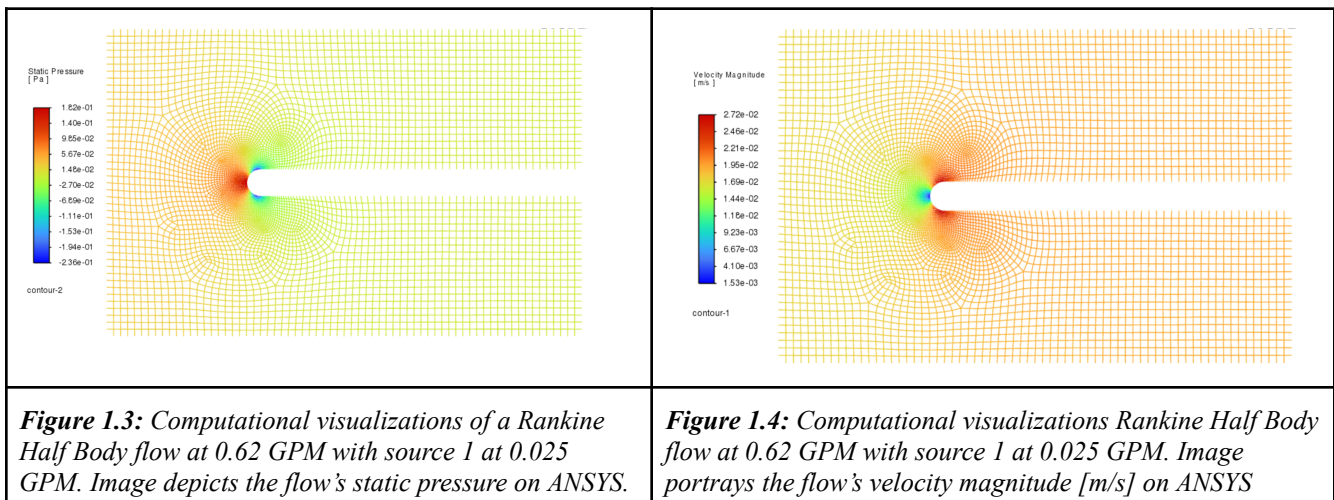


Figure 1.2: Computational visualization of a Rankine Half Body flow at 0.62 GPM with source 1 at 0.025 GPM. The image presents the analytical streamlines generated using ANSYS.



IV.5.3 Experimental Results (Image Processing) & Error Analysis

Based on the image processing done in MATLAB [A1], there was 0.0140 meters between the stagnation point and source 1. We can regard this distance as the value of negative x (indicating negative horizontal displacement) and utilize that to calculate the experimentally obtained source strength [A2]:

$$m = 2 \cdot \pi \cdot U \cdot x$$

where U is the uniform flow velocity we obtained from the part in IV.1 (0.0173 m/s).

$$m = 2\pi \cdot 0.0173 \cdot 0.0140 = 1.52 \cdot 10^{-3} \text{ m}^2/\text{s}$$

Using this result, we can conduct an error analysis between the source strengths found in IV.5.1 ($3.1546 \times 10^{-4} \text{ m}^2/\text{s}$) and here:

$$\text{Error (\%)} = \frac{1.52 \cdot 10^{-3} - 3.1546 \times 10^{-4} \text{ m}^2/\text{s}}{1.52 \cdot 10^{-3}} \cdot 100\% = 79.2\%$$

We have that the error between the analytically and experimentally obtained source strength is around 79.2%

IV.6 NACA 8612 Airfoil with and without leading edge slot

IV.6.1 Lift Analysis

The lift coefficient C_{L0} for the NACA 8612 airfoil was calculated using the theoretical equation:

$$C_{L0} = 2\pi(\alpha + 0.26)$$

where α represents the AoA in radians. The total lift force L generated by the airfoil was determined using the standard lift equation:

$$L = \frac{1}{2} \rho U^2 S C_{L0}$$

with ρ denoting the density, V the flow velocity, S the surface area, and C_{L0} the lift coefficient.

This formula represents how the airfoil performs under various flow conditions and AoAs, and assessing the stall characteristics.

The baseline tests without the slat indicated that stall occurred at a relatively lower AoA of around 45 degrees. The lift coefficient C_{L0} initially increased with the AoA until reaching a peak, beyond which a rapid decline was observed, marking the stall point.

The introduction of the leading-edge slat altered the stall characteristics significantly. The stall was delayed, allowing the airfoil to maintain higher C_{L0} values over a broader range of angles. This effect is attributed to the slat's ability to energize the boundary layer, enhancing its attachment to the airfoil surface at higher angles.

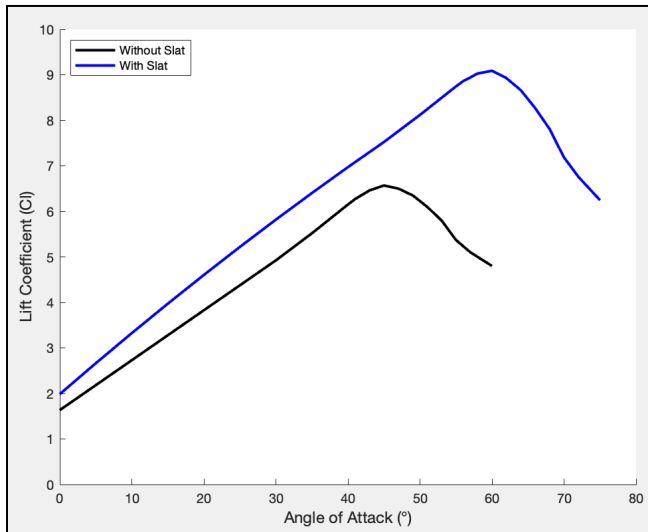
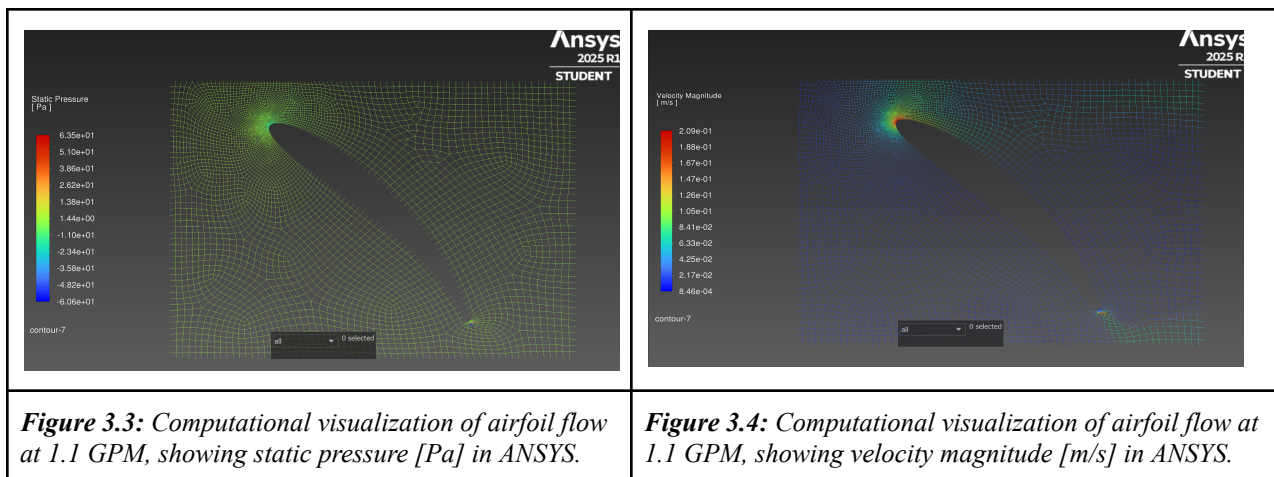
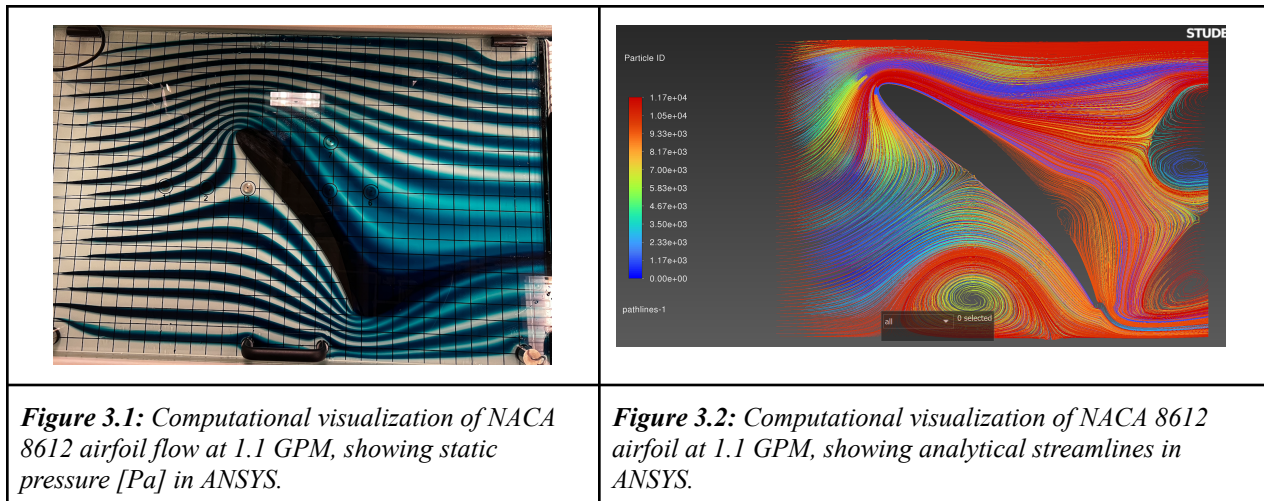


Figure 2: Comparison of lift Coefficient vs. Angle of Attack (AoA) for the NACA 8612 Airfoil with and without a leading-edge slat. The black curve represents the airfoil without the slat, showing an earlier stall at 40°. The blue curve represents the AoA of the airfoil with the slat, proving the slat's effectiveness by delaying the stall to 60°.

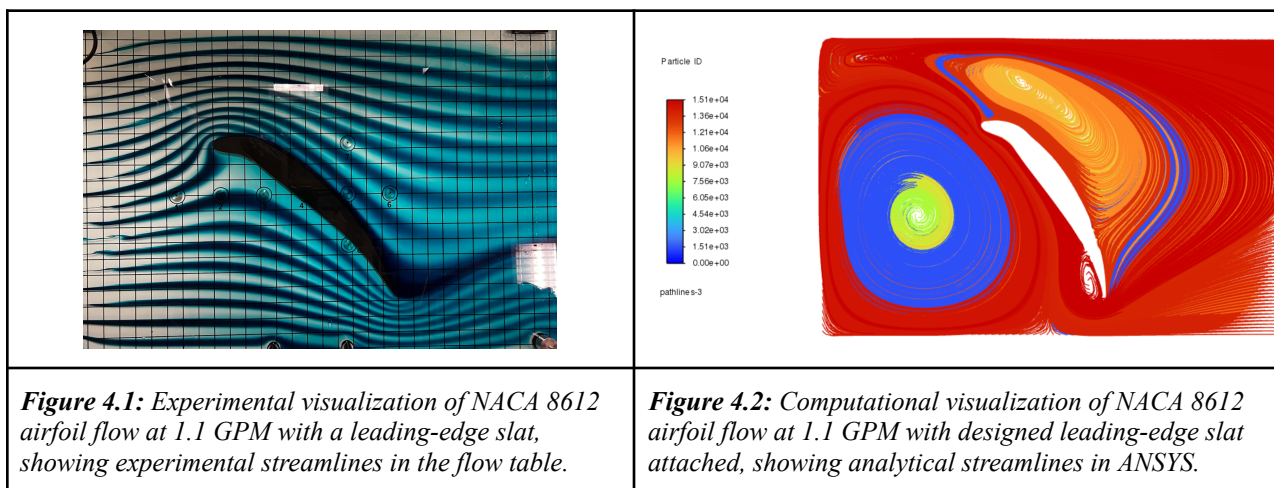
The experimental data [Fig. 2] was plotted to show the lift coefficient against the AoA for both configurations. The curves depict the stall point shift induced by the slat, affirming its efficacy in delaying stall. Numerical analysis provided additional insights into the flow behaviour around the airfoil and the slat, validating the experimental results.

IV.6.2 Airfoil without Edge Slat

The pathline visualization [Fig 3.2] shows significant flow separation on the upper surface, leading to the formation of large recirculation zones. This corresponds to the stall observed in the laboratory experiment [Fig. 3.1], where ink smudging indicated disrupted flow. The velocity contour plot [Fig. 3.4] reveals a sharp velocity gradient near the leading edge, with a low-velocity wake region forming behind the airfoil due to separation. The static pressure distribution [Fig. 3.3] demonstrates a region of high pressure at the stagnation point (leading edge), followed by a sharp pressure drop along the suction surface. The large adverse pressure gradient near the trailing edge leads to boundary layer detachment.

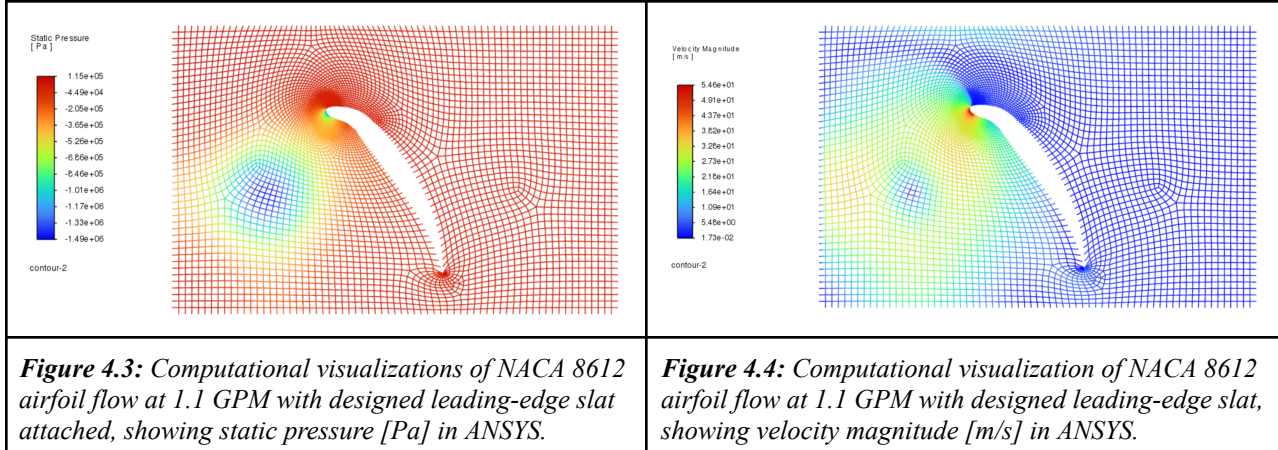


IV.6.3 Airfoil with Leading Edge Slat



The experimental and computational visualizations of the NACA 8612 airfoil with a leading-edge slat provide a clear demonstration of the slat's impact on flow behavior at 1.1 GPM. Figure 4.1 shows the

experimental streamline visualization, which illustrates how the leading-edge slat helps maintain smooth flow attachment along the airfoil's surface. This real-life observation confirms the slat's effectiveness in mitigating flow separation, a critical factor in delaying stall. Figure 4.2 further complements this by displaying the computational streamline analysis using ANSYS, where a marked reduction in flow separation can be seen compared to typical airfoil configurations without slats.



Additionally, Figures 4.3 and 4.4 provide a deeper insight into the flow's static pressure distribution and velocity magnitude, respectively. The static pressure visualization in Figure 4.3 highlights a region of high pressure at the leading edge, gradually decreasing along the surface, indicative of effective flow management by the slat. Meanwhile, Figure 4.4's velocity magnitude plot shows a uniform flow without significant disruptions, confirming the computational prediction of enhanced aerodynamic performance due to the slat. These visualizations not only validate the slat's design rationale but also underscore the potential for such modifications to significantly enhance airfoil efficiency in real-world applications.

V. DISCUSSION

The results obtained from the Hele-Shaw flow studies and the airfoil lift analysis offer valuable insights into the behavior of fluid flow around different bodies and the aerodynamic advantages of leading-edge modifications. The experimental observations closely align with theoretical predictions, though certain discrepancies highlight the complexities of real-world fluid mechanics.

The Hele-Shaw apparatus provided a clear visualization of how fluids behave around objects like cylinders and Rankine bodies. The flow around these objects displayed the classic characteristics predicted by potential flow theory, including the formation of stagnation points and symmetric flow fields. Specifically, the experiments effectively demonstrated how the geometry of an object influences its surrounding flow field, with the cylindrical and Rankine shapes producing different patterns. This is useful for validating theoretical models and improving design strategies in engineering applications.

While potential flow theory assumes an ideal, inviscid fluid, the real flow conditions observed tell a slightly different story. Minor deviations between theoretical and experimental streamline patterns suggest that viscous effects, though minimal, do influence the flow. This is evident from the discrepancies noted in the streamlined behavior around objects, where slight separations and vortices were observed despite the theory suggesting otherwise.

V.1 Reynolds Number Analysis Discussion

The calculated Reynolds numbers for different scenarios provided a quantitative backbone for our

observations. The table below summarizes these calculations, which confirm the laminar nature of the flow across all tested configurations, given the Reynolds numbers were well below the threshold for turbulence ($Re < 10^5$).

Table 1: Reynolds Number summary for four different scenarios

	Undisturbed Flow	Cylinder	Rankine-Half Body	Rankine-Full Body
Reynolds Number	86.068	1967.523	49.956	3904.061

V.2 Airfoil Performance with Leading-Edge Slat

Perhaps the most compelling part of our study was the analysis involving the NACA 8612 airfoil, where the introduction of a leading-edge slat significantly altered its stall characteristics. Experimentally, it allowed the airfoil to maintain higher lift coefficients at increased AoAs, effectively delaying onset of stall from 45 degrees to 60 degrees. This enhancement is attributed to the slat's ability to energize the boundary layer, improving the airfoil's aerodynamic efficiency by maintaining flow attachment over the wing surface for longer angles.

The airfoil simulation results are consistent with theoretical and experimental expectations. The stall condition is evident from the flow separation and wake formation in the high AoA (45°) case, which matches the laboratory observations of ink smudging and separation. The presence of vortex shedding in the wake region suggests turbulent unsteady behavior, which was not explicitly captured in the steady-state simulation but would be prominent in a transient analysis. The high adverse pressure gradient on the suction surface led to boundary layer detachment, confirming classical airfoil stall characteristics.

V.3 Rankine Half Body Simulation

The Rankine half-body simulation agrees with potential flow theory. The absence of separation and the smooth streamline behavior validate the superposition principle used in theoretical derivations. The pressure distribution closely resembles analytical solutions, confirming the suitability of inviscid approximations in this scenario.

V.4 Limitations

Our study assumes steady-state flow and neglects the potential impact of transient behaviors, which are particularly relevant at high angles of attack where flow dynamics rapidly change. Future experiments should aim to address these dynamics to better replicate operational conditions. The airfoil simulations assume steady-state flow, whereas real-world stall behavior is inherently unsteady and involves vortex shedding. The turbulence model choice may influence separation predictions, requiring further validation against experimental data. Additionally, Mesh refinement could impact wake resolution, particularly for the airfoil case.

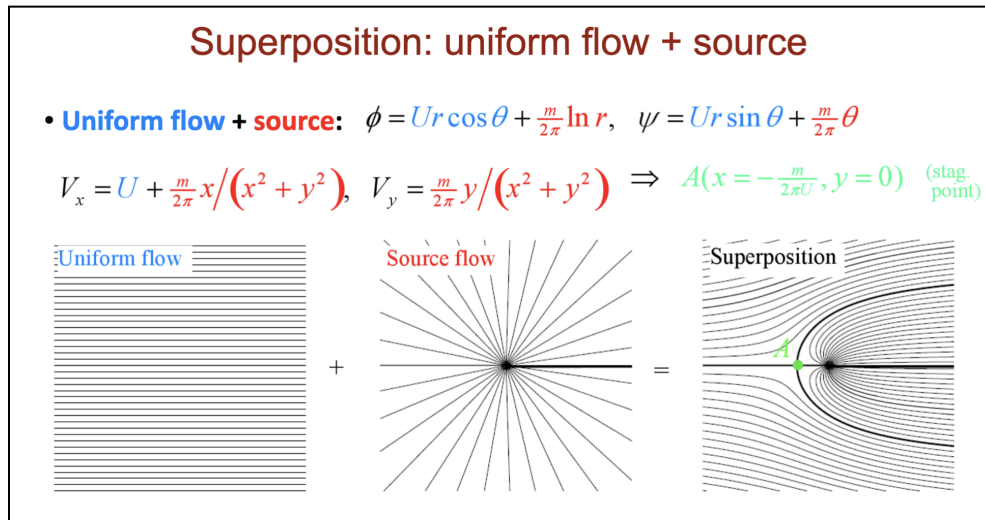
V.5 Conclusion

This study has provided valuable insights into the fluid dynamics of Hele-Shaw flow and the aerodynamic performance of airfoils with and without leading-edge slats. Through meticulous experimentation and detailed simulations, we have demonstrated how structural modifications can significantly influence flow behavior, enhancing our understanding of fluid mechanics principles and their practical applications. The introduction of a leading-edge slat on the NACA 8612 airfoil notably delayed stall and maintained higher lift coefficients, underscoring the potential for aerodynamic optimization in aircraft design. However, while the results affirm the utility of potential flow theory in predicting fluid behavior around streamlined bodies, they also highlight the limitations of this theory under real-world conditions where viscous and transient effects play a significant role. Future research should focus on incorporating these dynamic factors into simulations and experiments to achieve a more comprehensive understanding of fluid dynamics. By continuing to bridge the gap between theory and practice, we can better inform the design of more efficient and effective aerodynamic structures.

REFERENCES

- [1] Munson, B. R., Okiishi, T. H., Huebsch, W. W., & Rothmayer, A. P. (2021). *Fundamentals of fluid mechanics* (9th ed.). Wiley.
- [2] Smith, R. C., & Greenkorn, R. A. (1969, December 1). *An investigation of the flow regime for Hele-Shaw Flow*. OnePetro.
<https://onepetro.org/spejournal/article/9/04/434/164488/An-Investigation-of-the-Flow-Regime-for-Hele-Shaw>
- [3] Kleissl, J., De Callafon, R. (2025). *Potential flow*. MAE 171A.
- [4] ANSYS, Inc. (2023). ANSYS Fluent (Version 2023 R1). <https://www.ansys.com>

APPENDIX



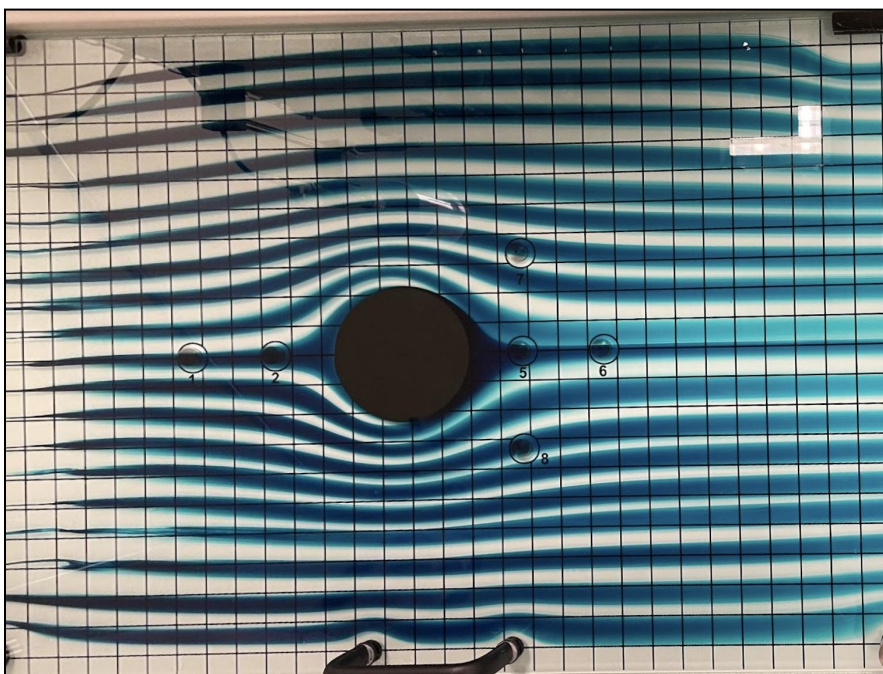
[A2] Description of Rankine Half-Body from MAE 171A Lecture notes

[A3] Assumptions

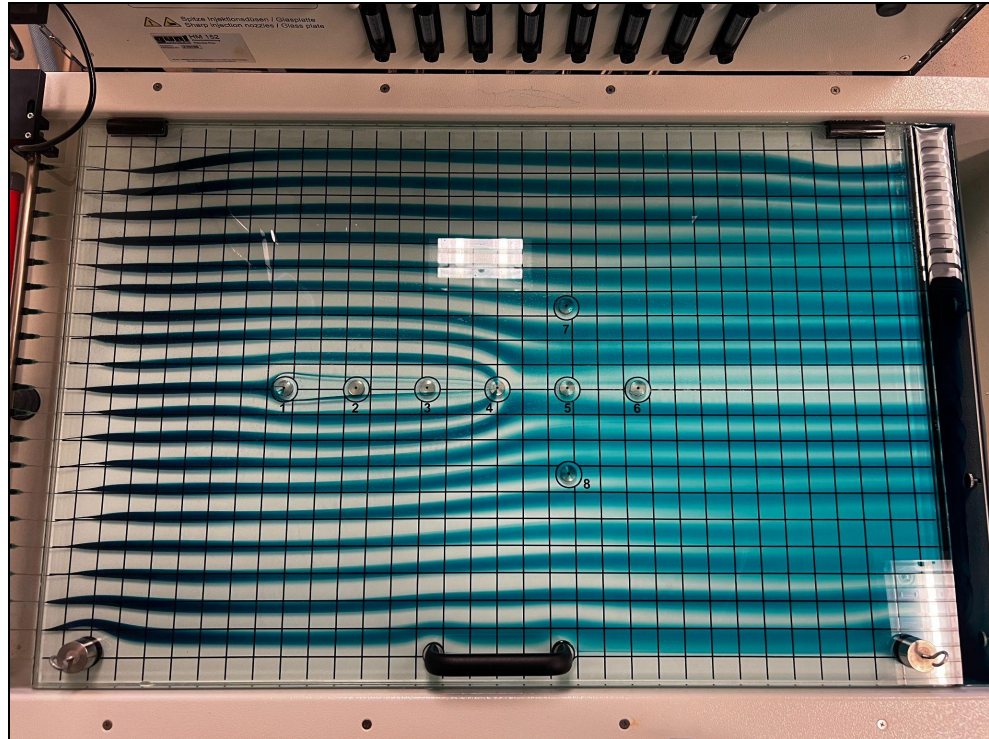
- Incompressible Flow: The flow is assumed to be incompressible due to the low Reynolds number and the nature of the Hele-Shaw setup.
- Steady-State Conditions: The flow is assumed to be steady, meaning that velocity and pressure distributions do not change with time.
- Two-Dimensional Flow: The Hele-Shaw apparatus constrains flow between two parallel plates, approximating a two-dimensional flow field.
- Negligible Viscous Effects (Potential Flow Assumption for Rankine Half-Body): The Rankine half-body experiment assumes an ideal inviscid fluid with no boundary layer effects. However, in reality, there is some viscosity present.
- Uniform Freestream Conditions: The main water flow is considered uniform before encountering obstacles, ensuring that variations in inlet velocity are minimal.
- Negligible End Effects: The finite dimensions of the experimental setup introduce edge effects, but these are assumed to be negligible in the central flow region.
- Constant Flow Rate: The flow rate is assumed to be constant throughout the experiment, controlled via the rotameter and maintained at 0.8 GPM.



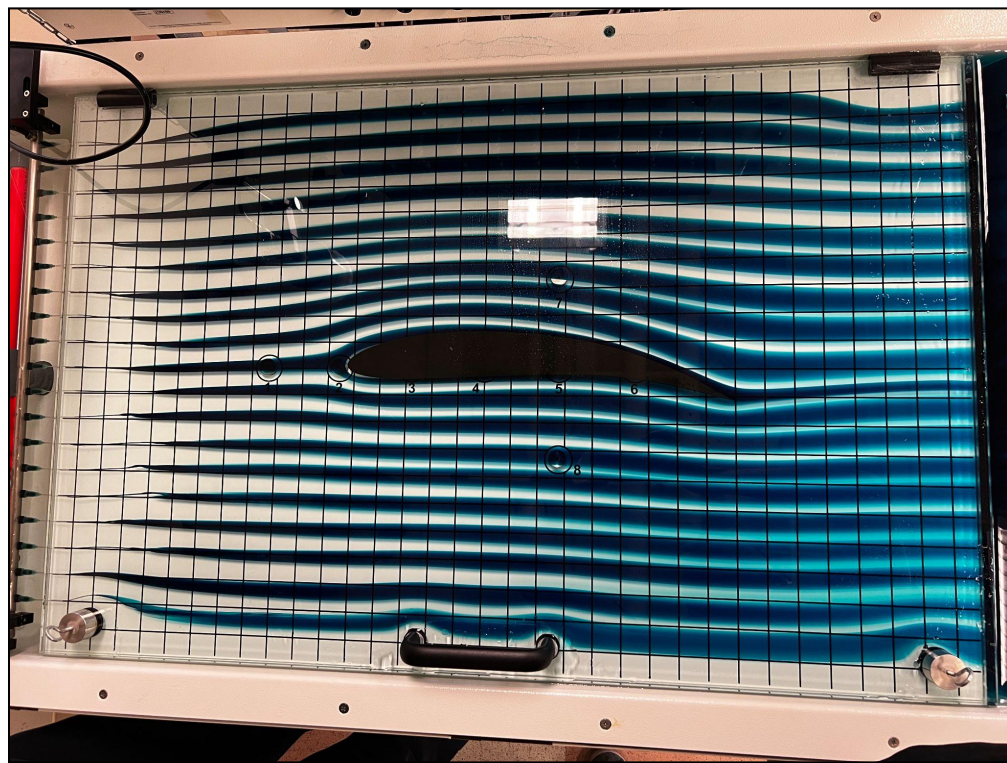
[A4] Undisturbed Flow



[A5] Flow with 4.5" cylindrical object



[A6] Rankine Full-Body Flow with source 1 and sink 4



[A7] Flow with Airfoil at 0 degrees

Individual Contributions

Alice: Performed Reynolds number calculations, lift analysis calculations and plot, and wrote figures' descriptions in the report.

Tanmay: Performed ANSYS simulations, wrote Theory, wrote Procedures. wrote part of discussion.

Ravi: Drafted airfoil CAD and performed ANSYS simulations, did image processing calculations, helped in results and discussion sections, and formatted the report.

Rayyan: Helped in simulations and calculations, and wrote the abstract and introduction section in the report.